Network Structure and Mechanical Properties of Sulfur-Cured Rubbers

M. Klüppel

Deutsches Institut für Kautschuktechnologie e.V., Eupener Strasse 33, D-30519 Hannover, FRG

G. Heinrich*

Continental AG, Materials Research/Tire Research, P.O. Box 169, D-30001 Hannover, FRG

*Received October 21, 1993; Revised Manuscript Received March 28, 1994**

ABSTRACT: The effect of sulfur/accelerator amount (at fixed ratio) and accelerator type (*n*-cyclohexylbenzothiazole-2-sulfenimide, diphenylguanidine) on network parameters (network chain density, cross-linking density, tube diameter, trapping factor) of styrene–butadiene copolymer networks is investigated via uniaxial stress–strain measurements up to large extensions. The mechanical properties are discussed in the framework of a non-Gaussian network model. It includes topological constraints for the network chains and the network junctions (cross-links and trapped entanglements). The model assumes a trapped entanglement contribution to the stress that does not vanish in the infinite strain limit. The two types of junctions (cross-links and trapped entanglements) are assumed to fluctuate in a Flory–Kästner domain around their mean position, while the chain segments fluctuate in a conformational tube built up by the surrounding chains. The finite extensibility component of the measured stress is evaluated by using a series expansion of the inverse Langevin function. The typical network parameters are estimated from the Gaussian contribution to the stress. It is found that the cross-link contribution G_c of the moduli changes approximately linearly with the concentration of cross-linking agent sulfur. Vanishing values of the moduli G_c are found at finite concentrations of cross-linking agent that are related to the gel point. The concentrations of cross-links at the gel points are almost identical for both systems of accelerators whereas the estimated cross-linking efficiencies are different. In relation to the estimated structure parameters, some measured technically important mechanical properties (tensile strength, hardness, rebound resilience, dynamic losses) of the differently accelerated sulfur-cured SBR networks are discussed qualitatively in the framework of the proposed network model.

1. Introduction

Considerable efforts have been undertaken in the past to study the effect of the cross-linking structure on the physical properties of vulcanized polymers. Especially, the static and dynamic properties of styrene–butadiene copolymer vulcanizes prepared with a sulfur/accelerator system, the most widely applied agent in the rubber industry, are of high technical importance. It implies the use of activators (zinc oxide and a fatty acid) and is employed with unsaturated rubbers. The relative percentage of the different structures in sulfur-cross-linked rubbers is a function of the initial sulfur/accelerator ratio. If it is greater than 2 (conventional system), it leads preferably to polysulfide structures. Below the value of 2, the so-called semi-efficient (semi-EV) and EV systems are built up, which basically give rise to mono- and disulfide structures.[1] Recent results have shown that vulcanizates with predominantly polysulfide cross-links exhibit properties (viz., tensile strength, modulus, and elongation at break) superior to those of the corresponding monosulfide cross-linking vulcanizates.[2] The effect of accelerator to sulfur ratio variation on the cross-linking density and on the rubber attachment on the filler surface of a carbon black filled styrene–butadiene elastomer was studied in ref 3.

The stress–strain behavior up to large extensions of natural rubber networks cured with tetramethylthiuram disulfide (TMTD) and dicumyl peroxide (DCP) was investigated in refs 4–7. From the observed differences between the two types of networks, it was concluded that chain scission occurs in the DCP-curing procedure, which leads to a reduced trapping rate of entanglements and, hence, to a smaller topological constraint contribution to the reduced stress (C_2 term of the Mooney–Rivlin equation). These conclusions are based on a network model which describes the stress–strain properties of topologically constrained amorphous rubber networks on the basis of non-Gaussian chain statistics.[8] The model includes topological constraints for the chains[9-12] as well as for the cross-links.[13,14] The influence of dangling chain ends is considered by using Scanlan's method of counting elastically effective strands,[15] which is closely related to the trapping of interchain entanglements.[16-18] The model allows the evaluation of the trapping factor from uniaxial stress–strain measurement data and leads to an extensive characterization of the network structure, including the fraction of elastically effective chains, trapped entanglements, cross-links, and chain scission probabilities during the curing procedure. The predictions of the model were found to be in good agreement with experimental results. Especially, the assumed contribution of trapped entanglements to the infinite strain modulus (C_1 term of the Mooney–Rivlin equation) and its relation to the consideration of the finite extensibility component of the reduced stress were demonstrated. Further, the influence of network swelling in the stress–strain data could be explained, even up to high swelling degrees.[7]

The aim of the present paper is to elaborate some more theoretical details and examine the interrelationships between the above-introduced model and some other theoretical predictions concerning rubberlike elasticity, e.g., the front factor. In addition, we study for the first time the effect of sulfur/accelerator amount (at fixed ratio) and accelerator type (*N*-cyclohexylbenzothiazole-2-sulfenimide (CBS), diphenylguanidine (DPG)) on network parameters of styrene–butadiene copolymer networks and their mechanical properties which play an important role under service conditions of the vulcanizates. The network

* Abstract published in *Advance ACS Abstracts*, May 15, 1994.

0024-9297/94/2227-3596$04.50/0

parameters (network chain density, cross-linking density, tube diameter, trapping factor) are estimated from well-established molecular models. We use the generalized tube model of rubber elasticity,[9-12] which was extended in refs 4–6 to the case of large extensions of rubber samples, where non-Gaussian statistics of the network chains occurs. The success of the tube model in the description of the mechanical properties of unfilled as well as filled elastomers prepared by statistical vulcanization of long primary chains has been demonstrated in refs 4–7, 12, and 19–26. It was shown that the tube model allows a proper separation of cross-link and other constraint contributions to the stress–strain behavior and a reliable determination of cross-linking densities. Further, it could be stated very recently that the tube approach with deformation-depedent constraints yields a very satisfactory description of the small-angle neutron scattering properties in the range of moderate deformations.[27]

2. Theoretical Part

2.1. General Assumptions. Our interpretation of stress–strain data is based upon the evaluation of a series expansion for the inverse Langevin function,[8] which allows the elimination of the finite extensibility contribution to the measured stress up to large deformations. We assume that trapped entanglements act in a stretched network similar to cross-links[13,28,29] and expect three different influences of constraints on a single strand between two cross-links. The first results from the cross-links themselves, which are allowed to fluctuate symmetrically in a spherical range built up by the surrounding chains.[13,14] The second influence is due to trapped entanglements of the strand under consideration, which act similarly to cross-links but differ in having a higher mobility compared to the cross-links only.[13] The third influence results from an additional reduction of chain fluctuations, caused by the surrounding chains, i.e., packing effects, which are assumed to build a constraining tube around every strand. These topological constraints are taken into account in the framework of Gaussian statistics only. They are related to a constraining potential for the chains, which is derived self-consistently in refs 9–11. All three influences are expected to be decoupled and contribute to the stress additively.[13] For uniaxial deformations this leads to the following series expansion for the reduced stress:[4,5]

$$\sigma_{red} = \frac{\sigma_0}{\lambda - \lambda^{-2}} = G_I\left\{1 + \frac{3}{25n}\left(3\lambda^2 + \frac{4}{\lambda}\right) + \frac{297}{6125n^2}\left(5\lambda^4 + 8\lambda + \frac{8}{\lambda^2}\right) + ...\right\} + G_N\frac{2(\lambda^{1/2} - \lambda^{-1})}{\lambda^2 - \lambda^{-1}} \approx G_I\{1 + ...\} + G_N\frac{1}{\lambda} \quad \text{for } \lambda \gtrsim 1 \quad (1)$$

where the infinite strain modulus G_I is given by

$$G_I = G_c + G_eT_e \quad (2)$$

σ_0 is the stress related to the cross section of the undeformed sample, λ is the deformation ratio in the direction of strain, G_c and G_e are moduli related to cross-links and entanglements, respectively, T_e is the Langley trapping factor for the entanglements,[16-18] G_N is the topological constraint modulus resulting from the Merseberg tube model,[9-12] and n is the mean number of statistical segments between successive junctions, i.e., cross-links or trapped entanglements. In terms of molecular quantities, it holds[4-6]

$$G_c = A_c\nu_ckT = \frac{A_c\hat{\nu}_s{l_s}^2kT}{\langle {R_0}^2\rangle_c} \quad (3)$$

$$G_e = A_e\nu_ekT = \frac{A_e\hat{\nu}_s{l_s}^2kT}{\langle {R_0}^2\rangle_e} \quad (4)$$

$$G_N = \frac{\hat{\nu}_s{l_s}^2kT}{4(6^{1/2}){r_0}^2} \quad (5)$$

and

$$n = \frac{\hat{\nu}_s}{\nu_c + \nu_eT_e} = \frac{\hat{\nu}_skT}{\frac{G_c}{A_c} + \frac{5}{4}{G_N}^0T_e} \quad (6)$$

Here, A_c and A_e are microstructure factors which are governed by the amount of fluctuations of cross-links and entanglements, respectively. ν_c and ν_e are the number densities of elastically effective strands which are related to cross-links and entanglements. k is the Boltzmann constant, T is the absolute temperature, and l_s is the length of statistical segments. G_N^0 is the plateau modulus of the un-cross-linked melt, $\langle R_0^2\rangle_e$ is the rms end-to-end distance between two successive entanglements in the melt, $\langle R_0^2\rangle_c$ is the rms end-to-end distance between two successive cross-links, and r_0 is the mean fluctuation radius (tube radius) of the chain segments in the undeformed network. The quantity $\hat{\nu}_s$ denotes the segment density of the elastically effective network, which is related to the segment density ν_s of the whole sample (including chain ends and sol molecules) via the trapping factor T_e and the gel fraction w_g. In the case of tetrafunctional cross-links, one finds[4-6]

$$\hat{\nu}_s = \left(\frac{3}{2}{T_e}^{1/2}w_g - \frac{T_e}{2}\right)\nu_s \quad (7)$$

A similar relation connects the density ν_c of elastically effective strands related to cross-links to the density of cross-links μ_c:[15-18]

$$\nu_c = (3Te^{1/2}w_g - T_e)\mu_c \quad (8)$$

These expressions take into account elastically ineffective chain ends but not ineffective closed loops, which may exist in statistically cured networks as well. This influence is neglected throughout the present paper.

2.2. Junction Fluctuations and Microstructure Factors. To clarify the structure of eq 2 for the infinite strain modulus and in view of evaluating the microstructure factors A_c and A_e, we briefly discuss some more details concerning the decomposition of the free energy of a network consisting of two types of junctions, cross-links and topologically fixed entanglements. The microstructure factors A_c and A_e in eqs 3 and 4 depend on the fluctuations of the two types of junctions. Starting from the assumed decomposition of the free energy of a network consisting of two types of junctions (cross-links and topologically fixed entanglements) and referring to the tensor formalism of Kästner,[13,14] who assumed fluctuating Gaussian chains but restricted symmetric junction fluc-

tuations, one can derive the following expression (Appendix):

$$A_c = \frac{1}{2} + \frac{1}{\pi^{1/2}}\left(\frac{K_c \exp(-K_c^2)}{\operatorname{erf} K_c}\right) \quad (9)$$

$$A_e = \frac{1}{2} + \frac{1}{\pi^{1/2}}\left(\frac{K_e \exp(-K_e^2)}{\operatorname{erf} K_e}\right) \quad (10)$$

with

$$K_c = 6^{1/2}\frac{r_c}{\langle R_0^2\rangle_{ce}^{1/2}} \quad (11)$$

$$K_e = 6^{1/2}\frac{r_e}{\langle R_0^2\rangle_{ce}^{1/2}} \quad (12)$$

$\langle R_0^2\rangle_{ce} = n l_s^2$ is the rms end-to-end distance between two successive junctions (trapped entanglements or cross-links) where $\langle ... \rangle_{ce}$ denotes the average over both types of chains. The length scales r_c and r_e characterize the range of the junction fluctuations. According to the Flory picture of restricted junction fluctuations,[30,31] the limiting case $r_c = r_e = 0$ corresponds to a total suppression of fluctuations ($A_c = A_e = 1$) and the case $r_c = r_e = \infty$ corresponds to the free-fluctuating limit ($A_c = A_e = {}^1/_2$ for tetrafunctional junctions). In the case of cross-links, the localization length r_c can be approximately identified with the tube radius r_0 ($r_c \approx r_0$). Then A_c can be evaluated by using eq 5 and it can be shown that in the case of moderately cross-linked networks $A_c \approx 0.67$ independent of cross-linking density (compare next section). The fluctuation radius of trapped entanglements r_e is expected to be larger than r_c by reason of the looser connectivity in comparison to cross-links. Therefore, from theoretical arguments the factor A_e is assumed to have a value of approximately ${}^1/_2$, which is the limiting value of eq 10 for large radii of fluctuations.

2.3. Scaling Relations. An important tool to test the predictions of a theory is its scaling relations, which reflect the inner structure of the theory in terms of experimentally detectable quantities. In the framework of the tube model, the following scaling relation between the tube radius r_0 and the segment density ν_s can be derived:

$$r_0 = \alpha(\nu_s l_s^3)^{(1-\kappa)/2} l_s \quad (13)$$

Various scaling pictures of polymer entanglements yield various exponents κ ($\kappa = 2, {}^7/_3$, and 3) as has recently been discussed by Colby et al.[32] Recent calculations on polymer melts, based on a mean field model for entanglements and assuming an extraordinary influence of packing effects, led to $\kappa = 2$ and $\alpha = \alpha_{melt} \approx 8.5$.[9-11] The value of the prefactor α_{melt} is almost identical to the value obtained by a least squares fit of experimental data in the Graessley–Edwards paper.[33] However, α could not be calculated with the necessary accuracy in the network case (the calculations gave $\alpha \approx 1$).[10] Therefore, α was determined by comparing theoretical results for the constraint contribution of the shear modulus with experimental values for some typical elastomers[12,34] and by neutron scattering experiments.[27] The quantity α was found to range between $\alpha = 2$ and $\alpha = 5$, dependent on the cross-linking density and the defects in the network.

An explanation of the observed variation of α in the case of networks is possible if relation 13 is combined with an empirical scaling relation, which assumes a linear dependence between the tube radius and the mean distance of successive junctions:[4-6]

$$r_0 = \frac{n^{1/2} l_s}{\xi} \quad (14)$$

Here ξ is a scaling factor, which was found from experimental data to have the value $\xi \approx 2$.[4-6] For networks with a large number of scission-induced defects, the value of ξ was found to be somehow smaller than 2. This correlates with the assumption that the constraining tubes are enlarged because of the dilution of the network by the chain ends.[4-6] A combination of eqs 13 and 14 with $\kappa = 2$ leads to

$$\alpha = \frac{(\nu_s l_s^3)^{1/2}}{\xi}\lambda_{max} \quad (15)$$

where the relation $\lambda_{max} = n^{1/2}$ for the limiting extensibility of the network is used. Equation 15 describes the influence of cross-linking density on the parameter α, because λ_{max} is a decreasing function of the number of cross-links. Typical values of λ_{max} lie between 3 and 5 (compare Table 2), while the reduced segment density $\nu_s l_s^3$ for most elastomers ranges between 2 and 5. Hence, the predictions of eq 15 fit well to the above-reported values of the prefactor α. Another useful scaling relation is found if eq 14 is combined with eqs 5 and 6. It yields

$$G_c = \frac{4(6^{1/2})A_c G_N}{\xi^2} - \frac{5}{4}A_c G_N T_e \quad (16)$$

By plotting G_c against G_N, one can use this relation to determine the trapping factor T_e from the axis intersection and the scaling factor ξ from the slope of the plot. The above-reported value $\xi \approx 2$ was found by using this procedure.[4-6]

The structure factor A_c can be evaluated from eqs 9, 11, and 14 if the relations $\langle R_0^2\rangle_{ce} = n l_s^2$ and $r_c \approx r_0$ are used. This yields $K_c = 6^{1/2}/\xi$, and with $\xi \approx 2$ we find $A_c \approx 0.67$, independent of cross-linking density. It should be noted that this was not found in refs 4–6, where larger values for A_c were used. However, the calculation of the finite extensibility component is not influenced by the value of A_c significantly. The main influence in eq 6 results from the number of trapped entanglements in the network, which is generally found to be significantly larger than the number of cross-links.

3. Materials and Procedures

Statistically polymerized styrene–butadiene copolymers (SBR 1500) with 23 wt % styrene were cured with two different sulfur/accelerator cross-linking systems at 150 °C, almost completely up to 95% of the maximum torque found in vulcameter measurements. The amount of cross-linking agent was varied systematically and different important ingredients were added. The ratio between sulfur and accelerator remained unchanged. The mixing composition of the different types of samples is listed in Table 1. In addition, the vulcanization times t_{95}, i.e., the time needed to reach 95% of the maximum torque found in vulcameter curves, are shown.

Uniaxial stress–strain properties of the samples were determined at room temperature by using strip probes. The extension ratios were measured by an optical system (Universalprüfmaschine Zwick 1445). To avoid dynamical contributions to the stress, the deformation velocity was chosen small enough (10 mm/min) that no significant influence of the velocity on the measured stress could be detected. Figure 1 shows a typical example of stress–strain curves (Mooney–Rivlin plots) found at a sample of type B_1. Besides the reduced stress, which is plotted

Table 1. List of Mixing Compositions and Optimal Curing Times t_{95} for the Different Sample Types[a]

	sample type					
	A_1	A_2	A_3	B_1	B_2	B_3
styrene–butadiene rubber (SBR 1500)	100	100	100	100	100	100
stearinic acid	2	2	2	2	2	2
zinc oxide	3	3	3	3	3	3
sulfur	2	4	6	2	4	6
accelerator: DPG[b]	0.8	1.6	2.4			
accelerator: CBS[c]				0.8	1.6	2.4
curing time t_{95}/min	140	115	60	40	25	20

[a] All numbers except curing times are weight units. [b] DPG: diphenylguanidine. [c] CBS: *N*-cyclohexylbenzothiazol-2-sulfenimide.

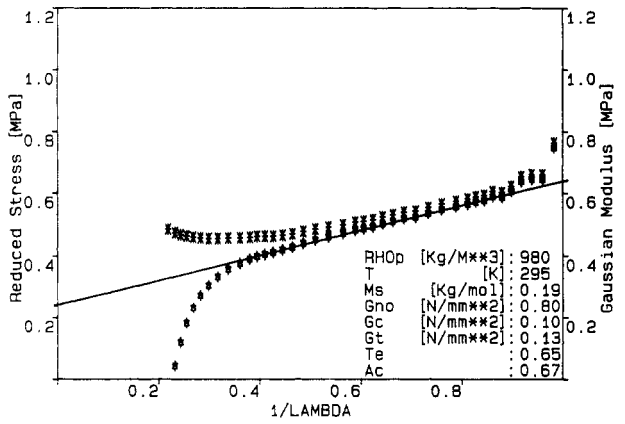

Figure 1. Mooney–Rivlin plot of the reduced stress and the calculated Gaussian contribution for a sample of type B_1.

against the inverse deformation ratio, the calculated Gaussian contribution to the reduced stress is shown. This contribution equals eq 1 when the first term, i.e., the one of the series expansion, is considered only. The calculation of the Gaussian contribution is performed by using eqs 1, 6, 7, and 16 and an iteration procedure for the determination of the moduli G_c and G_e as well as the trapping factor T_e. Details of this procedure are found in refs 4 and 5. The plateau modulus and the segment density of the un-cross-linked melt are found from dynamical measurements in refs 35 and 36, respectively, together with a weight-average mixing rule. It yields $G_N^0 = 0.8$ MPa and $\nu_s = \rho_p N_A/M_s = 3.1 \times 10^{27}$ m^{-3} ($\rho_p = 980$ kg/m^3 (mass density), N_A = Avogadro's number, and $M_s = 0.19$ kg/mol (molar segment mass)). The gel fraction of the networks is taken to be $w_g = 1$. All parameters which enter the calculation on the Gaussian contribution are listed in the legend of Figure 1.

In addition to the stress–strain properties, which are used for a determination of the structure parameters of the networks, some technically important network properties (tensile strength, elongation at break, hardness, rebound resilience, temperature dependence of loss tangent) were measured. In this way, we show and discuss a route to correlate basic network parameters with network properties which are important under service conditions. Hardness and rebound resilience are measured according to ASTM procedures. The loss tangent, i.e., the ratio between the loss and storage moduli, is measured with a dynamic mechanical tester (EPLEXOR tester[40]) in the compression mode of constant deformation (10% static deformation, 0.2% dynamic amplitude) and at a frequency of 10 Hz.

4. Results and Discussion

A typical result found from the Mooney–Rivlin plots of the examined SBR rubbers (Figure 1) is the linear dependence of the calculated Gaussian contribution on a large deformation scale. The systematic deviations of the calculated curve from the regression line at extremely large extensions are probably due to a rupture of single chains, while the deviations at small extensions can be related to an insufficient calibration between the zero of stress and

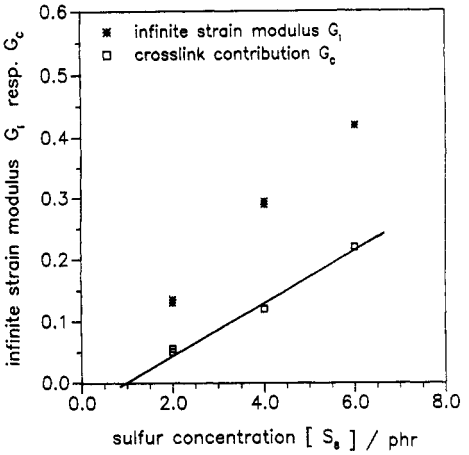

Figure 2. Plot of the infinite strain modulus and its cross-link contribution versus sulfur content for the sulfur/DPG-cured networks.

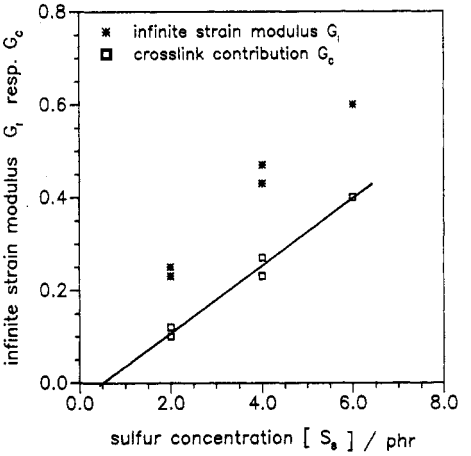

Figure 3. Plot of the infinite strain modulus and its cross-link contribution versus sulfur content for the sulfur/CBS-cured networks.

strain. According to eq 1, the regression line for the Gaussian contribution to the reduced stress determines the infinite strain modulus G_I and the topological constraint modulus G_N.

Figures 2 and 3 show plots of the infinite strain moduli G_I as a function of concentration of cross-linking agent sulfur for the two different systems, accelerated with DPG and CBS, respectively. In addition, the calculated moduli G_c are shown, which are assumed to change linearly with the concentration of cross-linking agent sulfur. The corresponding regression lines in Figures 2 and 3 demonstrate that a vanishing modulus G_c is found at finite concentrations of cross-linking agent (0.95 phr for the DPG-accelerated and 0.5 phr for the CBS-accelerated networks), which are related to the gel point of the cross-linking procedure. The different axis intersections for the two systems correspond to different cross-linking efficiencies μ_c/[sulfur] = 0.049 for the sulfur/DPG system and μ_c/[sulfur] = 0.083 for the sulfur/CBS system, respectively. Both values are found from the slope of the regression lines in Figures 2 and 3 by using eqs 3 and 8 and the limiting value 1 for the trapping factor T_e (see below). The concentration of cross-links at the gel point is almost identical for both systems ($\mu_{gel\ point} = 13.2$ mol/m^{-3} for the DPG-accelerated system and $\mu_{gel\ point} = 11.8$ mol/m^{-3} for the CBS-accelerated system).

The plots in Figures 2 and 3 clearly demonstrate the influence of trapped entanglements on the infinite strain modulus as stated by eq 2. The limiting contribution

Table 2. List of Network Parameters Found from Uniaxial Stress–Strain Measurements[a]

	sample type					
	A_1	A_2	A_3	B_1	B_2	B_3
T_e	0.4	0.85	1	0.65	1	1
n	19.9	11.1	9.5	13.7	9.2	7.9
λ_{max}	4.5	3.4	3.1	3.7	3.0	2.8
α	4.9	3.7	3.4	4.1	3.3	3.1
μ_c/[sulfur]		0.049			0.083	

[a] T_e = trapping factor; n = segment number between successive junctions; λ_{max} = limiting network extensibility; α = prefactor of eqs 13 and 15; μ_c/[sulfur] = cross-linking efficiency.

$G_eT_{e,max}$ of trapped entanglements is identified with the limiting difference $(G_I - G_c)$ at large concentrations of cross-linking agent sulfur. It is found to be equal for both types of networks ($G_eT_{e,max} \approx 0.2$ MPa). By assuming $T_{e,max} = 1$ (see below), the trapping factor T_e is found from the corresponding smaller contributions $(G_I - G_c)$ for all samples. These values are listed in Table 2 together with the number n of statistical segments between successive junctions, as found from eqs 6 and 7, the limiting extensibility of the network $\lambda_{max} = n^{1/2}$, and the prefactor α, which follows from eq 15 with a reduced segment density $\nu_s l_s^3 = 4.8$. (The segment length $l_s = 1.16$ nm is taken from refs 35 and 36 together with a weight-average mixing rule.) In addition, the cross-linking efficiencies for the two types of systems are listed in Table 2.

By using eq 4 and a common relation between the density of elastically effective strands ν_e and the plateau modulus $G_N°$ of a polymer melt $G_N° = {}^4/_5\nu_e kT$, it follows from the above experimental data that the microstructure factor A_e is significantly smaller than the theoretically expected limit $A_e = {}^1/_2$ as concluded in section 2.2. Instead, $A_e \approx 0.2$ results from $G_eT_{e,max} \approx 0.2$ MPa, $T_{e,max} = 1$, and $G_N° = 0.8$ MPa. The same result $A_e \approx 0.2$ was found in refs 4–6 for natural rubber samples cured with TMTD and DCP, respectively, which demonstrates the experimental significance of this value independent of polymer type and cross-linking agent. The discrepancy with the calculated value indicates that the theoretical description of fluctuations of trapped entanglements is insufficient at the present state. A possible reason for the observed deviation is the enlarged mobility of trapped entanglements resulting from the ability of the chains to slide across each other. This means that, contrary to the case of cross-links, the two segments that are linked are not fixed, which is also described by the alternative expression "sliplink" instead of entanglement. This property is not considered sufficiently in the calculations of the microstructure factor (see Appendix). As an alternative explanation for the observed deviation, it can also be imagined that entanglements slide onto each other or onto a cross-link under large deformations, which would reduce the number, and hence the effectivity, of trapped entanglements as well. However, this kind of effect should reduce not only the infinite strain modulus but also the topological constraint modulus. We will see below that this is not the case, but trapped entanglements contribute to topological constraints in the same number as determined from the plateau modulus $G_N°$ under the condition of small deformations.

Figure 4 shows a plot of the cross-link modulus G_c against the topological constraint modulus G_N for both types of networks which were cured with the different cross-linking systems sulfur/DPG and sulfur/CBS. In addition, corresponding values of SBR networks cured with different amounts of tetramethylthiuram disulfide (TMTD) are

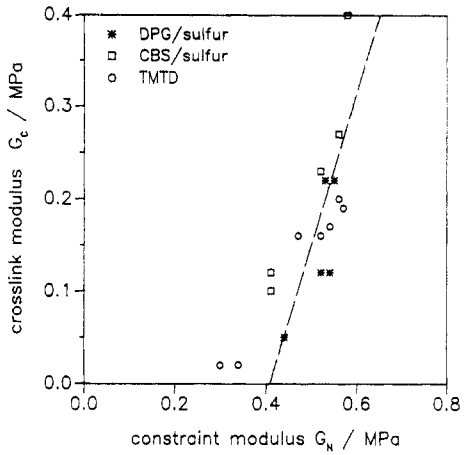

Figure 4. Plot of the cross-link cintrobution to the infinite strain modulus versus the topological constraint modulus for three different curing systems ((– – –) eq 16 with $G_N° = 0.8$ MPa, $\xi = 2$, and $A_c = 0.67$).

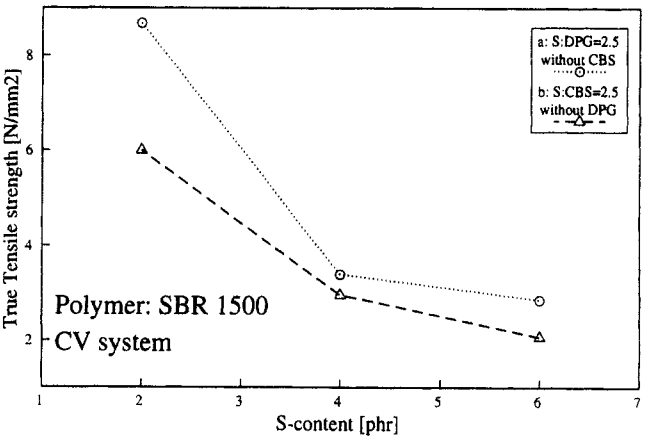

Figure 5. Plot of the true tensile strength versus sulfur content for the two different systems cross-linked with sulfur/DPG and sulfur/CBS.

shown. The inserted line corresponds to eq 16 with values $T_e = 1$, $\xi = 2$, $A_c = 0.67$, and $G_N° = 0.8$ MPa. The plot shows that the scaling eq 16 correlates well with experimental data for all three types of networks and that no reduction of trapped entanglements by the above-mentioned sliding effects at large deformations takes place. Contrary to earlier experimental data for peroxide-cured natural rubbers,[4–6] it is found that the limiting value of the trapping factor $T_{e,max}$ equals 1 in all three cases. This means that all entanglements in the rubber melt are trapped by the cross-links with increasing cross-linking density and no chain scission occurs in the curing procedures of SBR rubbers with the systems sulfur/DPG and sulfur/CBS and TMTD without sulfur.

In relation to the stress–strain properties, which are used for a determination of the structure parameters of the networks, additional mechanical data of the samples were obtained. Figures 5 and 6 show the ultimate properties of the SBR networks cured with sulfur/DPG and sulfur/CBS. It becomes obvious that the true tensile strength, i.e., the strength related to the cross section of the elongated samples, and the elongation at break are decreasing functions of the concentration of cross-linking agent sulfur. This means that the ultimate properties of the networks decrease with rising cross-linking density, which may result from the decreasing number of trapped entanglements in relation to the cross-links.[6] The generally larger ultimate values for the sulfur/DPG-cured samples correlate with this conclusion if the smaller cross-linking

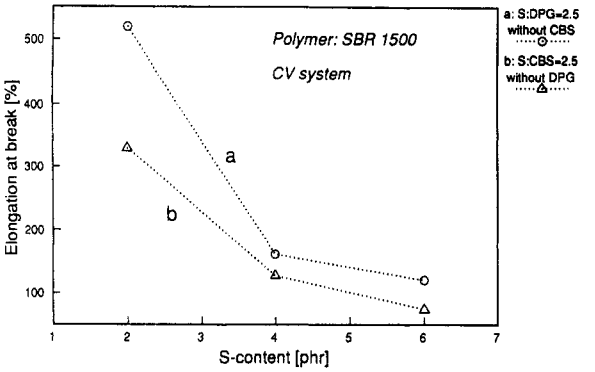

Figure 6. Plot of the elongation at break versus sulfur content for the two different systems cross-linked with sulfur/DPG and sulfur/CBS.

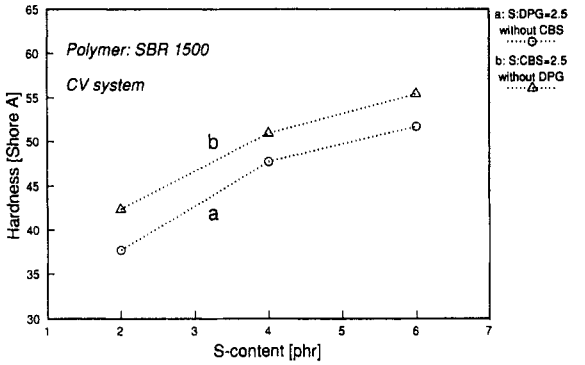

Figure 7. Plot of the hardness (Shore A) versus sulfur content for the two different systems cross-linked with sulfur/DPG and sulfur/CBS.

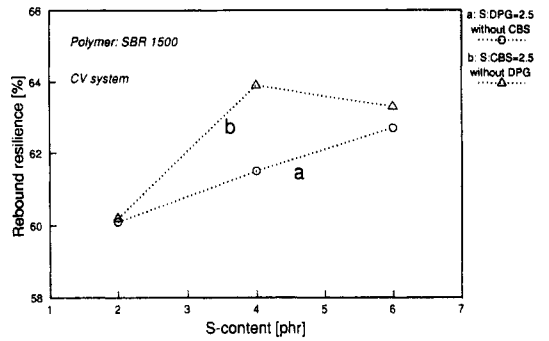

Figure 8. Plot of the rebound resilience versus sulfur content for the two different systems cross-linked with sulfur/DPG and sulfur/CBS.

efficiency compared to the sulfur/CBS-cured samples is considered (Table 2).

Of high technical importance for the studied SBR networks are the hardness and the rebound resilience of the samples. These properties were measured according to ASTM procedures. The results are shown in Figures 7 and 8. The detected rising hardness of the samples with sulfur content can directly be related to the increasing cross-linking density, which results in a reduction of mobility for the network chains. Similar to the ultimate properties, the observed difference between the two types of networks can be related to the different cross-linking efficiencies (Table 2). The measured rebound resiliences of the samples, which are shown in Figure 8, are found to be an increasing function of the cross-linking density. Obviously, this increase in resilience is due to a loss of long-time viscoelastic mechanisms with increased cross-linking.[41] However, this function passes through a maximum at high concentrations of cross-linking agent sulfur. This may be related to dynamical influences on the

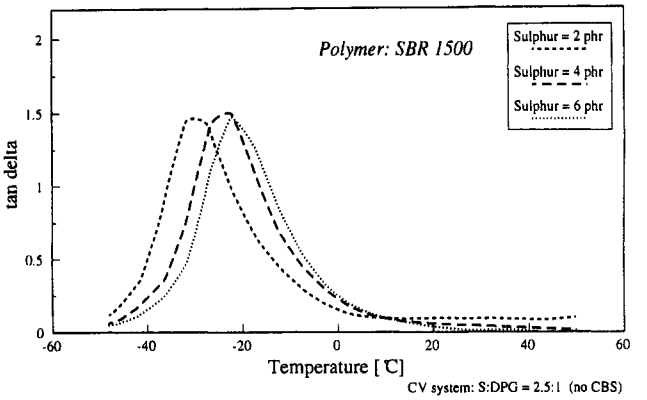

Figure 9. Plot of the dynamical loss ratio $G''/G' = \tan \delta$ versus temperature for three different sulfur concentrations (sulfur/DPG systems).

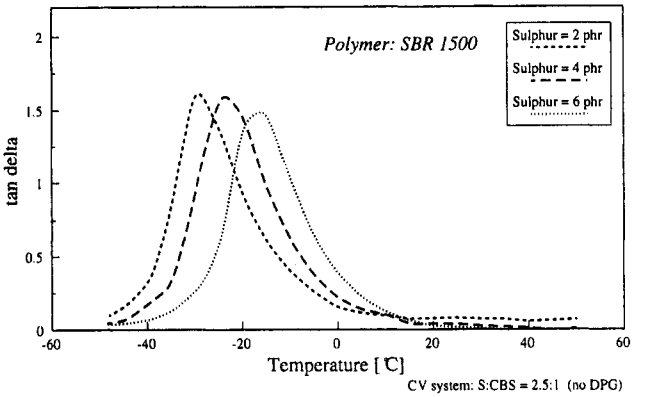

Figure 10. Plot of the dynamical loss ratio $G''/G' = \tan \delta$ versus temperature for three different sulfur concentrations (sulfur/CBS systems).

measurement values, which are not characterized in the present paper. Here, we will focus only on the influence of cross-linking density on dynamical losses in the glass transition range, which gives no significant effect on the rebound resiliences.

Figures 9 and 10 show the tangents of the loss angle, i.e., the ratio between the loss and storage moduli in oscillatory measurements, as a function of temperature for the two network types cured with sulfur/DPG and sulfur/CBS. The observed maxima refer to the transition of the networks from the glassy to the rubbery state. It becomes obvious that a shift of the glass transition temperature to higher temperatures results with increasing sulfur concentration. This is mainly due to the reduction of segment mobility by the cross-links but may also be related to a stiffening of the chains, which can result from the formation of cyclic sulfides at the chain backbones.[1] A closer examination of the origin of the observed glass transition shift is beyond the scope of the present paper.

5. Conclusions

In this paper, models of rubber elasticity are presented which include limiting chain extensibility, entanglements, and conformational packing effects. The models are applied to technically important rubber networks with different types of chemical cross-links. The results shown in Figures 2–4 confirm the extended tube model of networks proposed in the theoretical part of this paper and especially the scaling eq 14. It becomes obvious that the uniaxial stress–strain properties of the examined sulfur-cured SBR networks can be interpreted in analogy to the earlier-studied NR networks[4–7] on the basis of a trapped entanglement contribution to the infinite strain

modulus. Contrary to the case of DCP-cured NR networks, the limiting number of trapped entanglements, which is derived from the values of the topological constraint modulus, is found be in agreement with the number of entanglements in the un-cross-linked melt ($T_{e,max} = 1$). This means that no chain scission occurs in the cross-linking procedure of the examined SBR rubbers. The trapped entanglement contribution to the infinite strain modulus is found to be of nearly the same magnitude as the cross-link contribution (Figures 2 and 3), despite the larger number of trapped entanglements compared to the cross-links. This results from the lower microstructure factor and higher mobility of trapped entanglements compared to the cross-links. The larger number of trapped entanglements becomes dominant for the topological constraint modulus (Figure 4), because the mobility of the different junctions does not influence topological constraints significantly. For moderately cross-linked rubbers, an increasing ratio between cross-links and trapped entanglements with rising amount of cross-linking agent is observed which probably is related to the observed decreasing tensile strength properties of the samples with increasing cross-linking density (Figures 5 and 6).

We finally note that one may criticize the use of the inverse Langevin approximation and the tube constraints at the same time within the theoretical background of our investigations (eq 1) because (i) the tube concept is founded on Gaussian chain models[9-12] and (ii) the finite chain extensibility in networks comes at earlier deformations as predicted by the free chain.[42,43] However, we can argue that the action of tubelike constraints depends on the degree of network deformation and becomes weaker with increasing extensions, i.e., where finite chain extensibility becomes relevant.[44,45] Further, we point out that the Langevin approach is attributed to strands between chemical as well as physical elastically effective cross-links (trapped entanglements), and the relevant length scales of trapped entanglements and constraining packing effects are in the same order.

Appendix

The conformational energy (in units of kT) of a network consisting of M junctions is written in terms of the elements of the symmetric network connectivity (Kirchhoff) matrix as follows:

$$\sum_i \frac{3}{2\langle \mathbf{R}_{0i}^2\rangle}\mathbf{R}_i^2 = \sum_{m,n=1}^{M}\sum_{\mu=1}^{3}\gamma_{mn}x_{m\mu}x_{n\mu} \tag{A1}$$

Here, $\mathbf{R}_i$ denotes the end-to-end distance vector of the ith network chain and $\langle \mathbf{R}_{0i}^2\rangle$ is the rms distance of the equivalent isolated chain in the undeformed state of reference. The $\mathbf{x}_m$ ($m = 1, ..., M$) denote the vector positions of the junctions. The off-diagonal elements of the $M \times M$ reduced Kirchhoff matrix are[13,37]

$$\gamma_{mn} = \begin{cases} \dfrac{3}{2\langle \mathbf{R}_{0mn}^2\rangle} & \text{for junctions } m,n \text{ directly connected} \\ 0 & \text{otherwise} \end{cases} \tag{A2}$$

The diagonal elements are

$$\gamma_{mm} = -\sum_{n(\neq m)}\gamma_{mn} \tag{A3}$$

Following the line of Kästner,[13,14] we assume monodisperse network chains, i.e., $\langle \mathbf{R}_{0mn}^2\rangle = \langle \mathbf{R}_{0i}^2\rangle = \langle \mathbf{R}_0^2\rangle$ for all (m,n) or i. With the notation

$$\mathbf{x} = \bar{\mathbf{x}} + \Delta\mathbf{x} \tag{A4}$$

we find

$$\sum_{m,n}\sum_{\mu}\gamma_{mn}x_{m\mu}x_{n\mu} = \sum_{m,n}\sum_{\mu}\gamma_{mn}\bar{x}_{m\mu}\bar{x}_{n\mu} + \sum_{m,n}{}'\sum_{\mu}\gamma_{mn}\Delta x_{m\mu}\Delta x_{n\mu} + \sum_{m,n}{}'\sum_{\mu}2\gamma_{mn}\bar{x}_{m\mu}\Delta x_{n\mu} \tag{A5}$$

In eq A4 $\bar{\mathbf{x}}$ is the (time) averaged position vector of the junctions and $\Delta\mathbf{x}$ its fluctuation around $\bar{\mathbf{x}}$. The prime denotes that the summation is restricted over the mobile inner junctions, because junctions fixed at the border of the sample are assumed to possess zero fluctuations (James–Guth assumption[38]). The number of inner mobile junctions is on the order of the total number M. Therefore, we do not distinguish between these two numbers throughout this paper. It was shown in refs 38 and 13 that the last term of eq A5 vanishes if one assumes that the mean position $\bar{\mathbf{x}}_n$ coincides with the most probable values of $\mathbf{x}_n$, which determine the maximum of the network partition function. Then we obtain the following equation:

$$\sum_i \frac{3}{2\langle \mathbf{R}_{0i}^2\rangle}\mathbf{R}_i^2 = \sum_i \frac{3}{2\langle \mathbf{R}_{0i}^2\rangle}\bar{\mathbf{R}}_i^2 + \sum_{m,n}{}'\sum_{\mu}\gamma_{mn}\Delta x_{m\mu}\Delta x_{n\mu} \tag{A6}$$

Configurational averaging of eq A6 gives

$$\sum_i \frac{3}{2\langle \mathbf{R}_{0i}^2\rangle}\langle \mathbf{R}_i^2\rangle = \sum_i \frac{3}{2\langle \mathbf{R}_{0i}^2\rangle}\langle \bar{\mathbf{R}}_i^2\rangle + \sum_{m,n}{}'\gamma_{mn}\langle \Delta\mathbf{x}_m\Delta\mathbf{x}_n\rangle \tag{A7}$$

The undeformed state of reference is assumed to be the most probable state of a network chain with $\langle \mathbf{R}_i^2\rangle = \langle \mathbf{R}_{0i}^2\rangle$, which is sometimes called the Θ state.[39] Hence, we obtain

$$\frac{3}{2}N = \frac{3}{2}NA + \sum_{m,n}{}'\gamma_{mn}\langle \Delta\mathbf{x}_m\Delta\mathbf{x}_n\rangle \tag{A8}$$

where N is the number of network chains and A is the microstructure factor:

$$A = \frac{1}{N}\sum_{i=1}^{N}\frac{\langle \bar{\mathbf{R}}_i^2\rangle}{\langle \mathbf{R}_{0i}^2\rangle} = \frac{\langle \bar{\boldsymbol{R}}^2\rangle}{\langle \boldsymbol{R}_0^2\rangle} \tag{A9}$$

We note that the microstructure factor is equal to the front factor of the network:

$$g = \eta A = \frac{\langle \boldsymbol{R}^2\rangle}{\langle \boldsymbol{R}_0^2\rangle}\frac{\langle \bar{\boldsymbol{R}}^2\rangle}{\langle \boldsymbol{R}_0^2\rangle} \tag{A10}$$

because the memory term (or dilatation factor) of the network $\eta = \langle \boldsymbol{R}^2\rangle/\langle \boldsymbol{R}_0^2\rangle$ is equal to 1 (assumption of the Θ state).[13,39] Equations A8 and A9 yield the expression

$$A = 1 - \frac{2}{3N}\sum_{m,n}{}'\gamma_{mn}\langle \Delta\mathbf{x}_m\Delta\mathbf{x}_n\rangle \tag{A11}$$

Averaging about the fluctuations leads, after an orthogonal

transformation of the $\Delta\mathbf{x}_m$ and $\Delta\mathbf{x}_n$, to the expression[13,37]

$$\frac{1}{3}\sum_{m,n}{}'\gamma_{mn}\langle\Delta\mathbf{x}_m\Delta\mathbf{x}_n\rangle = \sum_m{}'\frac{\int_0^{K_m}x^2e^{-x^2}\,dx}{\int_0^{K_m}e^{-x^2}\,dx}$$
$$= \frac{M}{2} - \frac{1}{\pi^{1/2}}\sum_m{}'\frac{K_m e^{-K_m^2}}{\operatorname{erf} K_m} \quad \text{(A12)}$$

which gives

$$A = 1 - \frac{2}{f} + \frac{2}{N\pi^{1/2}}\sum_m{}'\frac{K_m e^{-K_m^2}}{\operatorname{erf} K_m} \quad \text{(A13)}$$

Here, erf x denotes the error function and $f = 2N/M$ is the average junction functionality, which is equal to 4 in the case of trapped entanglements and for most types of crosslinks. The quantity $K_m = r\gamma_m^{1/2}$ is related to the eigenvalue γ_m of the Kirchhoff matrix and to the length scale r which is available for mobile junctions to fluctuate about their mean position. The case $r = 0$ (total suppressed fluctuations) gives $A = 1$, and the limiting case $r = \infty$ (free-fluctuating limit) gives the famous James–Guth result $A = 1 - 2/f = {}^1/_2$.[38] In the following we replace the eigenvalues γ_m by their averaged values:

$$\bar{\gamma}_m = \frac{1}{M}\sum_{m=1}^{M}{}'\gamma_m \quad \text{(A14)}$$

Adapting the typical results of a regular network[13,37]

$$\gamma_m \approx \frac{2f}{3}\frac{3}{2\langle R_0^2\rangle}\sum_{\mu=1}^{3}\sin^2\left(\frac{m_\mu\pi}{2(M^{1/3}+1)}\right) \quad \text{(A15)}$$

with $m_\mu = 1, 2, \ldots, M^{1/3}$ and $\mu = 1, 2, 3$, we obtain the analytical approach:

$$K_m \to K = r\bar{\gamma}_m^{1/2} = \left(\frac{3f}{2}\right)^{1/2}\frac{r}{\langle R_0^2\rangle^{1/2}} \quad \text{(A16)}$$

and

$$A = \frac{1}{2} + \frac{1}{\pi^{1/2}}\frac{Ke^{-K^2}}{\operatorname{erf} K} \quad \text{(A17)}$$

in the case of tetrafunctional junctions with $f = 4$.

References and Notes

(1) Hofmann, W. *Rubber Technology Handbook*; Hanser Publishers: Munich, Vienna, New York, 1989.
(2) Nasir, M.; Teh, G. K. *Eur. Polym. J.* **1988**, *24*, 733.
(3) Spatis, G.; Kontou, E.; Saklabani, A. *J. Reinf. Plast. Compos.* **1991**, *10*, 391.
(4) Klüppel, M. *Prog. Colloid Polym. Sci.* **1992**, *90*, 137.
(5) Klüppel, M. *Kautsch. + Gummi, Kunstst.* **1993**, *46*, 197.
(6) Klüppel, M. *J. Appl. Polym. Sci.* **1993**, *48*, 1137.
(7) Klüppel, M. *Macromolecules*, submitted.
(8) Treloar, L. R. G. *The Physics of Rubber Elasticity*, 3rd ed.; Clarendon Press: Oxford, 1985.
(9) Heinrich, G.; Straube, E. *Acta Polym.* **1983**, *34*, 589; **1984**, *35*, 115.
(10) Heinrich, G.; Straube, E. *Polym. Bull.* **1987**, *17*, 247.
(11) Heinrich, G.; Straube, E. *Makromol. Chem., Macromol. Symp.* **1989**, *30*, 223.
(12) Heinrich, G.; Straube, E.; Helmis, G. *Adv. Polym. Sci.* **1988**, *85*, 33.
(13) Kästner, S. *Colloid Polym. Sci.* **1981**, *259*, 499, 508.
(14) Kästner, S. *Polymer* **1978**, *20*, 1327; *Acta Polym.* **1980**, *31*, 444.
(15) Scanlan, J. *J. Polym. Sci.* **1960**, *43*, 501.
(16) Langley, N. R. *Macromolecules* **1968**, *1*, 348.
(17) Langley, N. R.; Polmanteer, K. E. *J. Polym. Sci., Polym. Phys. Ed.* **1974**, *12*, 1023.
(18) Flory, P. J. *Chem. Rev.* **1944**, *35*, 51.
(19) Gottlieb, M.; Gaylord, R. J. *Polymer* **1983**, *24*, 1644.
(20) Higgs, P. G.; Gaylord, R. J. *Polymer* **1990**, *31*, 70.
(21) Vilgis, T. A. Polymer Networks. In *Comprehensive Polymer Science*; Pergamon Press: Oxford, England, 1989; Vol. 6.
(22) Oppermann, W.; Rennar, N. *Prog. Colloid Polym. Sci.* **1987**, *75*, 49.
(23) Matzen, D.; Straube, E. *Colloid Polym. Sci.* **1992**, *270*, 1.
(24) Straube, E.; Heinrich, G. *Kautsch. + Gummi, Kunstst.* **1991**, *44*, 734.
(25) Douglas, J. F.; McKenna, G. B. The Localization Model: Review and Extension to Rubber Elasticity. In *Elastomeric Polymer Networks*; Mark, J. E., Erman, B., Eds.; Prentice-Hall: Englewood Cliffs, NJ, 1992; p 327. McKenna, G. B.; Gaylord, R. J. *Polymer* **1988**, *29*, 2027.
(26) Heinrich, G.; Vilgis, T. A. *Macromolecules* **1993**, *26*, 1109.
(27) Straube, E.; Urban, V.; Pyckhout-Hintzen, W.; Richter, D. *Macromolecules*, submitted.
(28) Dusek, K.; Prins, W. *Adv. Polym. Sci.* **1969**, *6*, 102.
(29) Graessley, W. W. *Adv. Polym. Sci.* **1974**, *16*, 3.
(30) Flory, P. J. *J. Chem. Phys.* **1977**, *66*, 5720.
(31) Flory, P. J.; Erman, B. *Macromolecules* **1982**, *15*, 800.
(32) Colby, R. H.; Rubinstein, M.; Viovy, J. L. *Macromolecules* **1992**, *25*, 996.
(33) Graessley, W. W.; Edwards, S. F. *Polymer* **1981**, *22*, 1329.
(34) Helmis, G.; Heinrich, G.; Straube, E. *Wiss. Z. Tech. Hochsch. Leuna-Merseburg* **1984**, *26*, 461.
(35) Aharoni, S. M. *Macromolecules* **1983**, *16*, 1722; **1986**, *19*, 426.
(36) Brandrup, J.; Immergut, E. H., Eds. *Polymer Handbook*, 2nd ed.; Wiley-Interscience: New York, 1975.
(37) Eichinger, B. E. *Macromolecules* **1972**, *5*, 496.
(38) James, H. M.; Guth, E. *J. Polym. Sci.* **1947**, *4*, 153; *J. Chem. Phys.* **1943**, *11*, 455.
(39) Staverman, A. J. *Adv. Polym. Sci.* **1982**, *44*, 73.
(40) Ghaddum, V. F. *Kunststoffberater* **1991**, *7*, 8.
(41) Ferry, J. D. *Viscoelastic Properties of Polymers*, 3rd ed.; John Wiley & Sons, Inc.: New York, 1980.
(42) Edwards, S. F.; Vilgis, T. A. *Rep. Prog. Phys.* **1988**, *51*, 243.
(43) Edwards, S. F.; Vilgis, T. A. *Polymer* **1987**, *27*, 483.
(44) Heinrich, G.; Beckert, W. *Prog. Colloid Polym. Sci.* **1992**, *90*, 47.
(45) Kovac, J.; Crabb, C. C. *Macromolecules* **1986**, *19*, 1744.